10-1-2008

Sex differences in angiotensin signaling in bulbospinal neurons in the rat rostral ventrolateral medulla

Gang Wang
Weill Cornell Medical College

Teresa A. Milner
Weill Cornell Medical College; The Rockefeller University

Robert C. Speth
University of Mississippi, rs1251@nova.edu

Andrea C. Gore
University of Texas, Austin

Di Wu
University of Texas, Austin

See next page for additional authors

AMERICAN JOURNAL OF PHYSIOLOGY
REGULATORY, INTEGRATIVE AND COMPARATIVE PHYSIOLOGY

Am J Physiol Regul Integr Comp Physiol. 2008 Oct; 295(4): R1149–R1157. PMCID: PMC2576084
Published online 2008 Aug 6. doi: 10.1152/ajpregu.90485.2008: 10.1152/ajpregu.90485.2008 PMID: 18685065

Sex differences in angiotensin signaling in bulbospinal neurons in the rat rostral ventrolateral medulla

Gang Wang,[1] Teresa A. Milner,[1,2] Robert C. Speth,[3] Andrea C. Gore,[4] Di Wu,[4] Costantino Iadecola,[1] and Joseph P. Pierce[1]

[1]Division of Neurobiology, Department of Neurology and Neuroscience, Weill Cornell Medical College, New York; [2]Harold and Margaret Milliken Hatch Laboratory of Neuroendocrinology, The Rockefeller University, New York, New York; [3]Department of Pharmacology, University of Mississippi School of Pharmacy, University of Mississippi, University, Mississippi; and [4]Division of Pharmacology and Toxicology, University of Texas, Austin, Austin Texas

Address for reprint requests and other correspondence: J. P. Pierce and G. Wang, Division of Neurobiology, Weill Cornell Medical College, 411 East 69th St., New York, NY 10021 (e-mail: jppierc@med.cornell.edu; gaw2001@med.cornell.edu)

Received 2008 Jun 9; Accepted 2008 Jul 29.

Abstract

Sex differences may play a significant role in determining the risk of hypertension. Bulbospinal neurons in the rostral ventrolateral medulla (RVLM) are involved in the tonic regulation of arterial pressure and participate in the central mechanisms of hypertension. Angiotensin II (ANG II) acting on angiotensin type 1 (AT_1) receptors in RVLM neurons is implicated in the development of hypertension by activating NADPH oxidase and producing reactive oxygen species (ROS). Therefore, we analyzed RVLM bulbospinal neurons to determine whether there are sex differences in: *1*) immunolabeling for AT_1 receptors and the key NADPH oxidase subunit p47 using dual-label immunoelectron microscopy, and *2*) the effects of ANG II on ROS production and Ca^{2+} currents using, respectively, hydroethidine fluoromicrography and patch-clamping. In tyrosine hydroxylase-positive RVLM neurons, female rats displayed significantly more AT_1 receptor immunoreactivity and less p47 immunoreactivity than male rats ($P < 0.05$). Although ANG II (100 nM) induced comparable ROS production in dissociated RVLM bulbospinal neurons of female and male rats ($P > 0.05$), an effect mediated by AT_1 receptors and NADPH oxidase, it triggered significantly larger dihydropyridine-sensitive long-lasting (L-type) Ca^{2+} currents in female RVLM neurons ($P < 0.05$). These observations suggest that an increase in AT_1 receptors in female RVLM neurons is counterbalanced by a reduction in p47 levels, such that ANG II-induced ROS production does not differ

between females and males. Since the Ca^{2+} current activator Bay K 8644 induced larger Ca^{2+} currents in females than in male RVLM neurons, increased ANG II-induced L-type Ca^{2+} currents in females may result from sex differences in calcium channel densities or dynamics.

Keywords: C1 neurons, reactive oxygen species, NADPH oxidase, calcium channel, estrogen

THERE IS INCREASING EVIDENCE that sex differences contribute to the risk of cardiovascular disease, including hypertension (14, 44). Under the age of 45 yr, fewer women than men die from cardiovascular disease (1), a pattern which is reversed after menopause (52). Similar sex-associated differences exist in animal hypertension models: females develop hypertension later, and less severely, than males (11, 35, 62). Studies in humans and animal models indicate that central nervous system pathways play a critical role in the development and maintenance of hypertension (27). Specifically, increases in sympathetic nerve activity and changes in arterial baroreflex function are strongly implicated in the pathogenesis of the disorder. The rostral ventrolateral medulla (RVLM) contains tonically active presympathetic bulbospinal neurons, most of which express tyrosine hydroxylase (TH) [the C1 cell group (39)]. RVLM bulbospinal neurons are essential for the maintenance of sympathetic vasomotor tone (15, 16). In light of the involvement of tonic sympathoexcitation in hypertension, it is important to determine whether the RVLM bulbospinal pathway displays sex-associated anatomical or functional differences, which could support differences in cardiovascular vulnerability.

Angiotensin II (ANG II) plays a key role in the central regulation of hypertension (38). In particular, injection of ANG II into the RVLM increases sympathetic nerve activity and blood pressure (3, 17), actions that are mediated through angiotensin type 1 (AT_1) receptors. AT_1 receptors are expressed in the RVLM at high levels in humans (16) and low-to-moderate levels in rats (2, 8, 9). ANG II exerts some of its effects through the modulation of Ca^{2+} currents (57, 58, 64). Furthermore, the production of reactive oxygen species (ROS) by NADPH oxidase has emerged as critical in the mediation of the effects of ANG II (53, 63). Binding of ANG II to AT_1 receptors leads to the phosphorylation of the cytoplasmic NADPH oxidase subunit p47, inducing the production of ROS (21). Intracerebroventricular infusion of ANG II significantly increases ROS production in the RVLM (10), and the resulting increased sympathetic activity can be attenuated by NADPH oxidase inhibition (7). Additionally, oxidative stress and ROS production in the RVLM have been shown to directly contribute to the neural mechanisms of hypertension in stroke-prone spontaneously hypertensive rats (26) and two-kidney one-clip rats (34).

Because most studies are conducted on male animals, it is not known whether there are sex differences in AT_1 receptor signaling and ROS production in RVLM bulbospinal neurons. Therefore, these neurons were analyzed to determine whether there are sex differences in: *1*) immunolabeling for the AT_1 receptor and the key NADPH oxidase subunit p47 and *2*) the effects of ANG II on ROS production and Ca^{2+} currents.

MATERIALS AND METHODS

Animals. All experiments were approved by the Institutional Animal Care and Use Committees at Weill Cornell Medical College and the University of Texas at Austin. Postnatal *days 20* (P20) and *23* (P23) Sprague-Dawley rats were purchased from Charles River Laboratories (Wilmington, MA), and 4- and 12-mo-old Sprague-Dawley rats were purchased from the Animal Resource Center, University of Texas at Austin (originally obtained from Harlan, Indianapolis, IN).

To examine more directly the role of estrogen, all young adult (4 mo) and middle-aged (12 mo) female rats received bilateral ovariectomies (OVX) under isoflurane anesthesia (2% in oxygen), followed by estrogen replacement using a standard protocol (13). In particular, 4 wk after OVX, rats were subcutaneously implanted with Silastic brand capsules (Dow Corning, Midland, MI) (1.0 cm for young and 1.5 cm for middle-aged animals) under isoflurane anesthesia, containing 17β-estradiol (5% in cholesterol; the OVX+E group) or vehicle (100% cholesterol; the OVX+V group) for 3 days prior to perfusion. Different Silastic capsule implant lengths were used to account for differences in body weights (6). Although serum estradiol levels in these animals could not be measured for technical reasons, other studies from one of our labs show that these capsules result in physiologically relevant circulating estradiol concentrations (13).

Materials and antibodies. ANG II, Bay K 8644, nifedipine, pronase, and thermolysin were purchased from Sigma-Aldrich (St. Louis, MO). Losartan was a gift from Merck and DuPont (Whitehouse Station, NJ). Mn(III)tetrakis(4-benzoic acid)porphyrin chloride (MnTBAP) was purchased from Calbiochem (San Diego, CA). The peptide gp91ds-tat was synthesized by Bio-Synthesis (Lewisville, TX). l-ACSF containing 0.01% BSA was used as a vehicle for peptides, including ANG II and gp91ds-tat. DMSO was used as a vehicle for all other drugs. Rhodamine green was purchased from Lumafluor (Naples, FL). The fluorescent dye dehydroethidium was purchased from Molecular Probes (Eugene, OR). Antibodies to the AT_1 receptor [rabbit, No. 92578 (20)], p47 (goat, C-20, sc-7660; Santa Cruz Biotechnology, Santa Cruz, CA), and TH [mouse, No. 22941, Immunostar (12)] have been extensively characterized and localized in fixed rat brain tissue.

Electron microscopic immunocytochemistry. Methods for dual-label immunoelectron microscopy are described in detail previously (42, 43, 58) and are summarized here. Male and female rats (P23; 4- and 12-mo-old) were anesthetized with pentobarbital sodium (150 mg/kg ip) and transcardially perfused with 3.75% acrolein and 2% paraformaldehyde in 0.1 mol/l phosphate buffer (pH 7.4). Brains then were blocked and postfixed, and coronal sections were cut on a Vibratome (40 μm). Random systematic series of sections (1:12), through the RVLM from each animal, were then processed to immunoperoxidase (ImP) label (18) TH (1:20,000 dilution) and immunogold (ImG) label either the AT_1 receptor (1:200) (P23; 4- and 12-mo-old tissue) or p47 subunit (1:100) (P23 tissue), after a 48 h incubation. TH-ImP labeling was used since it can easily identify even the smallest, most distal dendritic processes of C1 neurons (59). Tissue sections were processed in two runs (1st run: P23 tissue; 2nd run: 4- and 12-mo-old tissue) with the tissue in each run being processed in parallel. For electron microscopy, sections were postfixed in 2% osmium, dehydrated, and embedded in Embed 812 (EMS, Hatfield, PA). One randomly selected RVLM section containing C1 TH-labeled processes per animal was then further processed for ultrastructural analysis. The C1 area of RVLM was defined as corresponding to levels 62–63 (anterior to posterior = −12.50 to −12.68 from bregma) of Swanson (55). The subregion selected for analysis was caudal to the facial nucleus, rostral to the A1 region (47), ventral to the nucleus ambiguus, and

flanked by the inferior olive, spinal trigeminal tract, and ventral surface of the medulla. Selected subregions were excised, glued onto blocks, and sectioned on a Leica UCT ultratome to generate thin sections (70 nm) that were collected on copper mesh grids. Grids were counterstained with uranyl acetate and Reynold's lead citrate prior to examination on a Tecnai electron microscope (FEI, Hillsboro, OR).

Electron microscopic data analysis. For each animal, electron microscopy grids were examined to determine which contained thin sections that passed through the surface of the Vibratome tissue section (thus containing a plastic/tissue interface), and one such grid was randomly selected for analysis. The plastic/tissue interface was then mapped onto an image of a randomly selected thin section from that grid, and grid squares adjacent to the interface that displayed undamaged morphology (i.e., were complete) were identified and numbered. One of these grid squares was randomly selected, and all TH-ImP-labeled dendritic profiles [identified by being postsynaptic to presynaptic terminals (37)] in it, and five adjacent fields (moving clockwise along the interface) were examined to determine total AT_1 or p47 immunogold particle number colabeling the dendritic profiles. This approach limited analysis to the most superficial portions of the tissue (0.1–1 μm from the surface), which displayed the most robust labeling, and ensured that a comparable tissue depth would be examined for all animals (41, 42, 50). Other ultrastructural processes were also identified following the criteria of Peters et al. (37), such as glial profiles, which tend to be long and thin, and are often interposed between pre- and postsynaptic structures, in a manner that conforms to their shape. Since preembedding ImG labeling techniques employing antibody dilutions comparable to those used in this study generate extremely low levels of nonspecific, background labeling [estimated to be 3% of all ImG labeling, based on control tests involving omission of the primary antibody (61)], all ImG particles colabeling TH-positive dendrites were counted. Comparisons were only made between experimental groups whose tissue was fixed with the same batch of fixative and processed in parallel in the same run to control for potential differences in fixation, dilutions, and incubation times between runs. Images were captured with a digital camera (AMT, Danvers, MA) and figures were assembled in Photoshop.

Retrograde labeling of RVLM neurons. The methods used to retrogradely label RVLM neurons are identical to previous descriptions from our laboratory (59, 60). P20 rats were anesthetized with isoflurane (2% in oxygen), rhodamine-microbeads were microinjected bilaterally into the spinal cord at T_2-T_4, and 2–3 days later, the P20 rats were killed. The brain stems were removed, immersed in an ice-cold, oxygenized sucrose, artificial cerebrospinal fluid [ACSF (58, 60)] and sectioned coronally into 300–400 μm slices using a Vibratome. These slices were incubated at 35°C in: *1*) a lactic acid (l)-ACSF (59, 60) with 0.02% pronase for 1 h, and *2*) an oxygenated l-ASCF (22) with 0.02% thermolysin for 1 h. To dissociate RVLM neurons, the region was first identified under an E600 fluorescence microscope by the presence of dye-labeled neurons, was then punched out, and the tissue stirred in 1-ASCF. Dissociated neurons were then immediately moved to petri dishes. Rhodamine-labeled neurons were identified using an inverted fluorescent Nikon Diaphot 300 microscope with brief ultraviolet light exposure.

Immunolabeling of isolated RVLM neurons. As described (57), isolated cells were fixed with 4% paraformaldehyde, permeabilized, blocked in 5% donkey serum, and incubated in a primary antibody cocktail of either: *1*) 1:2,000 TH + 1:100 AT_1 antisera, or *2*) 1:2,000 TH + 1:100 p47 antisera

for 1 h. Neurons were then incubated in a secondary antibody cocktail of either: *1*) 1:50 FITC-conjugated anti-mouse (J60618) + 1:100 Cy5-conjugated anti-rabbit (J71063) antisera, or *2*) 1:50 FITC-conjugated anti-mouse (J60618) + 1:100 Cy5-conjugated anti-goat (J72031) immunoglobulin for 1 h (Jackson ImmunoResearch, West Grove, PA), and visualized using the inverted microscope. Since it is not feasible to conduct immunolabeling on isolated cells after the whole cell patch-clamp process, these studies were conducted on a separate group of cells.

Patch-clamp recordings of isolated RVLM neurons. Whole cell patch-clamp recording of RVLM neurons was performed with an Axoclamp-2A amplifier with pClamp Window 8.0 (Molecular Devices, Sunnyvale, CA) as previously described (57, 58, 60). To determine whether ANG II affected cell currents, patched neurons were exposed to either vehicle (0.01% BSA in l-ASCF) or other drugs and then ANG II in vehicle (continuously for at least 10 min) or other drug-containing buffers by using a custom-designed double-barrel perfusion system. Using 2 mmol/l Ca^{2+} as a charge carrier, the voltage-gated Ca^{2+} channel currents were elicited by depolarization from a holding potential of −60 mV, which is close to the resting potential, to stepping potentials ranging from −50 mV to +20 mV. The current signals were filtered at 2 kHz, digitized online at a sampling rate of 10 kHz, and stored for later computer analysis using pClamp.

Detection of intracellular ROS. ROS production was assessed using dehydroethidium as an indicator (25, 59). Isolated neurons were incubated in 5 μmol/l dehydroethidium for 30 min and then exposed throughout the measurement to 5 μmol/l dehydroethidium-containing buffer. Time-resolved fluorescence was measured every 30 s by using an ethidium bromide filter and IPLab software (Scanalytics, Fairfax, VA). This sampling rate enabled us to accurately detect the initial phase of ANG II-induced ROS production, since the effects of ANG II on ROS production and Ca^{2+} currents occurred within 2 min. Recordings commenced when a stable baseline was achieved with vehicle (0.01% BSA in l-ASCF) or other drugs and then ANG II in vehicle. In all experiments, concurrent vehicle recordings were performed until there was no difference in dehydroethidium fluorescence intensity before ANG II application.

ROS and Ca^{2+} current data analysis. The amplitude of whole cell Ca^{2+} currents at the end of the 500-ms depolarizing pulse was measured as the amplitude of the L-type Ca^{2+} current; the amplitude of the transient component of the Ca^{2+} current was obtained by subtracting the amplitude of L-type Ca^{2+} currents from that of peak transient Ca^{2+} currents measured at 30 ms following initiation of depolarization pulses (59). ROS data are expressed as the ratio Ft/Fo, where Ft is fluorescence following the application of ANG II in a given cell, and Fo is the baseline fluorescence of the same cell immediately before application of ANG II (57).

Statistical analysis. An EC_{50} was obtained from the equation $y = \min + (\max - \min)/[1 + (x/EC_{50})^{Hillslope}]$ SigmaPlot software (SPSS Science, Chicago, IL), where y is the percentage of normalized maximal dehydroethidium intensity at a given ANG II concentration x. The statistical significance between two groups was analyzed by using either the Student's t-test, or ANOVAs. P values < 0.05 were considered significant. Values were reported as means ± SE, with N = animal number and n = data point number or cell number.

RESULTS

Female TH RVLM neurons display significantly more AT_1 and less p47 than males. Similar to previous light microscopic studies (46, 59) the RVLM of P23, 4- and 12-mo-old females and male rats all contained numerous TH-labeled neurons with extensive dendritic processes (Fig. 1*A*). These TH-ImP-labeled processes also were identifiable at the ultrastructural level (Fig. 1, *B* and *C*), and often contained AT_1-ImG (Fig. 1*B*) or p47 ImG (Fig. 1*C*) labeling. AT_1-ImG labeling was also observed in glial processes (Fig. 1*B*) and non-TH-positive dendrites, and much less frequently in presynaptic processes and vascular endothelial cells. P47-ImG labeling also was frequently observed in non-TH-positive dendrites, glial processes, presynaptic processes (Fig. 1*C*), and endothelial cells.

Analysis of all TH-labeled dendrites in randomly selected fields (18,150 μm^2 per animal) of TH-AT_1 dual-labeled P23 material revealed that, on average, the dendrites of P23 females contained significantly higher levels of AT_1-ImG labeling than those of males [2.6 ± 0.1 ImG particles/dendritic profile (ImGP/D) vs. 1.9 ± 0.2 ImGP/D, *t*-test, $P = 0.03$, $N = 6$, $n = 318$] (Fig. 2*A*). Comparable data was obtained from the tissue of both young (Y; 4 mo) and middle-aged (M; 12 mo) animals, processed in parallel to allow the application of a two-way ANOVA with sex and age as factors. TH-labeled RVLM dendrites in females (F) had significantly higher levels of AT_1-ImG labeling than in males (M) [$F(1,14) = 9.53$, $P = 0.008$], while there were no significant differences relating to age [$F(1,14) = 0.003$, $P > 0.05$] (YF: 2.0 ± 0.4 ImGP/D, $n = 319$; YM: 0.8 ± 0.1 ImGP/D, $n = 181$; MF: 1.8 ± 0.3 ImGP/D, $n = 347$; MM: 0.97 ± 0.03 ImGP/D, $n = 187$) (Fig. 2*B*). Additionally, OVX+E females had higher levels of AT_1-ImG labeling than OVX+V females [$F(1,8) = 5.80$, $P = 0.04$], while there was no significant difference relating to age [$F(1,8) = 0.22$, $P > 0.05$] (YOVX+E: 2.6 ± 0.5 ImGP/D, $n = 159$; YOVX+V: 1.3 ± 0.1 ImGP/D, $n = 160$; MOVX+E: 2.0 ± 0.5 ImGP/D, $n = 178$; MOVX+V: 1.53 ± 0.09 ImGP/D, $n = 169$) (Fig. 2*B*). Examination of TH-labeled dendrites in TH-p47 dual-labeled P23 tissue revealed that the dendrites of females contained significantly lower levels of p47-ImG labeling than those of males (0.7 ± 0.1 ImGP/D vs. 1.3 ± 0.1 ImGP/D, $P = 0.01$, $N = 6$, $n = 237$).

Thus, across the population of TH-labeled RVLM neurons AT_1 receptor-ImG labeling is present at higher levels in females than males. This sex difference can be observed in the prepubertal juvenile and persists into young adulthood and midlife. In adult females, estrogen also appears to enhance AT_1 receptor-ImG labeling, with higher levels observed in OVX+E vs. OVX+V tissue. In contrast, p47 subunit immunolabeling is present at lower levels in P23 females compared with P23 males. These lower levels are also observed in adulthood (40).

ANG II induces ROS production in RVLM bulbospinal neurons of female rats. Next, the effect of ANG II on ROS production and Ca^{2+} currents within individually identified bulbospinal neurons (7) was examined in dissociated RVLM neurons from female rats. To verify that these isolated neurons also express TH, AT_1, and p47, immunofluorescent labeling was used (Fig. 1, *D* and *E*). Examination of retrogradely transported rhodamine in parallel with either TH and AT_1 (Fig. 1*D*) or TH and p47 (Fig. 1*E*) labeling indicated that substantial portions of the neurons used in these studies contained TH, p47, and AT_1. The effect of ANG II on ROS production was then explored. In vehicle-treated neurons, ethidium bromide fluorescence intensity, reflecting ROS production, re-

mained stable during the monitoring period (not shown). ANG II induced an increase in the ROS signal in RVLM bulbospinal female neurons within 2 min of application, in a dose-dependent manner (EC_{50} = 89.2 nmol/l, Fig. 3*A*). The effect was first observed at 10 nmol/l (5 ± 1%; $P < 0.05$; n = 5) and reached a maximal effect at 1,000 nmol/l (25.3 ± 4.4%; $P < 0.05$; n = 5) (57, 58). A comparable dose response curve was established for male RVLM bulbospinal neurons (EC_{50} = 98.7 nmol/l, Fig. 3*B*). Fig. 4*A* shows a representative image of 100 nmol/l ANG II-induced ROS production in a rhodamine-labeled bulbospinal neuron. The increase in ROS induced by ANG II (100 nmol/l) was blocked ($P > 0.05$ vs. control) by the ROS scavenger MnTBAP (30 μmol/l; n = 6), the AT_1 receptor antagonist losartan (10 μmol/l; n = 4) and the NADPH oxidase peptide inhibitor gp91ds-tat (1 μmol/l; n = 7) (Fig. 4*B*). However, pretreatment with the AT_2 receptor antagonist PD123319 (30 μmol/l) did not inhibit ANG II-induced ROS ($P > 0.05$; n = 5). These data indicate that ANG II induces ROS production in RVLM neurons of female rats via AT_1 receptors and NADPH oxidase.

ANG II increases L-type Ca^{2+} currents of female RVLM bulbospinal neurons via AT_1 receptors and NADPH oxidase. NADPH oxidase-derived ROS are implicated in the increase of Ca^{2+} currents elicited by ANG II (21, 53). ANG II (100 nmol/l) enhanced the L-type component of the Ca^{2+} current in female RVLM bulbospinal neurons ($P < 0.05$; n = 6). This component was enhanced by the L-type Ca^{2+} channel activator Bay K 8466 (1 μmol/l; $P < 0.05$; n = 4) and blocked by nifedipine (1 μmol/l; $P < 0.05$; n = 4), indicating that it was a dihydropyridine-sensitive L-type current (Fig. 5*D*). In contrast, ANG II (100 nmol/l) did not affect the amplitude of transient components of the Ca^{2+} current in rat bulbospinal neurons of females (99.6 ± 3.4%, $P > 0.05$, n = 6). The increase in the L-type Ca^{2+} current induced by ANG II (100 nmol/l) was blocked ($P > 0.05$ vs. vehicle) by either losartan (10 μmol/l; n = 4) or gp91ds-tat (1 μmol/l; n = 4) (Fig. 5, *A*–*C*). These observations indicate that the ANG II-mediated increase in L-type Ca^{2+} currents in female bulbospinal neurons is dependent on AT_1 receptors and NADPH oxidase. Female RVLM neurons not displaying retrograde label, i.e., nonbulbospinal projecting, did not exhibit significant ANG II-induced Ca^{2+} currents ($P > 0.05$; n = 4; Fig. 6) as bulbospinal projecting neurons did ($P < 0.05$; n = 5).

ANG II-induced L-type Ca^{2+} currents, but not ROS production, are greater in females than in males. We then compared ANG II-induced effects on ROS production and L-type Ca^{2+} currents between female and male RVLM bulbospinal neurons. The increase in ROS signals induced by ANG II (100 nmol/l) was comparable in bulbospinal neurons of male and female rats (Figs. 3 and 7*A*) ($P > 0.05$; n = 5). ANG II increased the ROS signal in male RVLM bulbospinal neurons in a dose-dependent manner, which did not differ from that seen in females (males: EC_{50} = 98.7 nmol/l; females: EC_{50} = 89.2 nmol/l, Fig. 3). However, the increase in L-type Ca^{2+} currents induced by ANG II (100 nmol/l) was significantly larger in females than in males (Fig. 7*B*; $P < 0.05$; n = 6). Losartan (10 μmol/l) was equally effective in blocking increases in ANG II-induced ROS and L-type Ca^{2+} currents in males (L-type Ca^{2+} currents: control = 100 ± 0%; losartan + ANG II = 102.5 ± 1.5%; $P > 0.05$; n = 5; ROS: control = 1.0 ± 0.01; losartan + ANG II = 1.04 ± 0.018; $P > 0.05$; n = 4) and females (Fig. 5), indicating that the ROS and Ca^{2+} current changes are AT_1 receptor-dependent in both sexes. Thus, while ANG II induces similar levels of ROS production in female and male bulbospinal neurons, the increase in the L-type Ca^{2+} current is larger in females (Fig. 7, *A* and *B*). To determine whether there were differences in the voltage-gated Ca^{2+} influx independent of AT_1 receptors in both sexes, losartan was continuously used to block AT_1 receptors, so that the direct ef-

fect by Bay K 8644 (1 μmol/l) on L-type Ca^{2+} currents in RVLM neurons could be revealed. The Bay K 8644-induced Ca^{2+} current was also significantly larger in females than in males (Fig. 7*C*; $P < 0.05$; $n = 9$). Sex differences in ANG II-induced Ca^{2+} currents therefore appear to result from differences in the density or dynamics of L-type Ca^{2+} channels.

DISCUSSION

These findings demonstrate that *1*) female P23 rats display more AT_1 receptor-ImG labeling and less NADPH oxidase subunit p47-ImG labeling in TH-labeled RVLM neurons, compared with male rats, *2*) the elevated levels of AT_1 receptor-ImG labeling in females persist into adulthood and midlife, and *3*) AT_1 receptor-ImG labeling was higher in estradiol than in vehicle-treated OVX females. Additionally, in isolated RVLM bulbospinal neurons, ANG II induced comparable ROS production in female and male rats, an effect mediated by AT_1 receptors and NADPH oxidase. However, in these neurons ANG II triggered more pronounced L-type Ca^{2+} currents in females than in males. Female neurons also exhibited larger Ca^{2+} currents in response to the L-type Ca^{2+} channel activator Bay K 8644.

Our immunocytochemical studies examined the TH-positive C1 cell group (4) in the RVLM, while our neurophysiological studies examined RVLM bulbospinal neurons. Since C1 neurons represent 50 to 70% of all RVLM bulbospinal neurons (39, 54, 56) these two populations overlap extensively. The C1 cell group was selected for anatomical analysis because TH-ImP labeling can be readily observed in the smallest, most-distal C1 dendritic processes (59), allowing an examination of AT_1 and p47 labeling in the full dendritic arbors of these cells. In contrast, the use of retrograde transport techniques to identify RVLM bulbospinal neurons would have produced ultrastructural immunolabeling in only large proximal dendrites (33). Although anti-dopamine-β-hydroxylase-saporin studies have shown that the C1 cell group is not essential for the RVLM-mediated maintenance of resting sympathetic vasomotor tone, they do contribute to it and play a substantial role in cardiovascular regulation through involvement in several sympathoexcitatory reflexes (30, 49).

Some of our neuroanatomical and all of our neurophysiological observations were obtained in juvenile rats (P23). It is feasible to patch-clamp dissociated RVLM neurons from young animals. In the adult, one cannot either dissociate RVLM neurons or patch-clamp them in slices, because of more extensive myelination (28). At this age, however, rats are in a prepuberal state and sex hormones have not reached mature levels (45, 51). Therefore, observed sex differences in AT_1 receptors, p47, and Ca^{2+} currents at P23 cannot be fully ascribed to sex hormones, raising the possibility that genomic organization differences between males and females play a role. But, one cannot rule out that the low levels of sex hormones present at this early age could also be involved (45, 51). Estradiol pretreatment can affect ANG II-induced changes in intracellular Ca^{2+} concentration ($[Ca^{2+}]_i$) in cultured area postrema neurons isolated at P10 to P16 (36), although the effect observed in this group of cells is a reduction in the ANG II-induced increase in $[Ca^{2+}]_i$.

To directly test whether differences in AT_1 receptor-ImG labeling could also be observed at later time points when sex hormones play a greater role, tissue from young adult (4 mo) and middle-aged (12 mo) rats were analyzed. Furthermore, the OVX rat model, with the addition of either estradiol or vehicle, was used to overcome the difficulty of interpreting data in intact females, that

are under the influence of fluctuations in estradiol concentrations across the estrous cycle. Comparable sex differences were observed at both ages, suggesting that the characteristics of AT_1 signaling described in this study could persist into adulthood and middle age, when hypertension is more prevalent (32). We have reported similar reductions in p47-ImG labeling in TH-labeled RVLM neurons in adult females (40), indicating that these prepuberal differences can also be observed in adulthood. Additionally, analysis of adult females also allowed an exploration of the potential role of estrogen in modulating AT_1 receptor levels in the RVLM. Consistent with findings in other systems (23), the presence of estrogen (in OVX+E tissue vs. OVX+V tissue) appeared to have a significant effect on AT_1 receptor-ImG labeling. Analysis of p47-ImG labeling in TH-labeled RVLM neurons in adult females (40) did not reveal any significant changes across the estrous cycle.

AT_1 receptors and NADPH oxidase-derived ROS play a key role in the central mechanisms of hypertension (10, 53, 57, 58, 64). The fact that AT_1 receptor-ImG labeling was increased and p47-ImG labeling was decreased in TH-labeled RVLM neurons from female rats raises the possibility of a compensatory balance between AT_1 receptors and NADPH oxidase subunits, aimed at maintaining constant levels of ROS production. Consistent with this hypothesis, ANG II-induced ROS production in dissociated RVLM neurons did not differ between females and males. ROS production was attenuated by the AT_1 receptor inhibitor losartan and by the NADPH oxidase peptide inhibitor gp91ds-tat, attesting to the fact that ROS production was mediated by AT_1 receptors via NADPH oxidase. In addition, other factors could be involved in the apparent compensation observed in females. For example, AT_2 receptors, which have effects on ROS production opposite to those of AT_1 receptors (5) could also be upregulated. Furthermore, the ANG II-derived peptide Ang-(1-7), which can counteract the effects of ANG II, might also be involved (48). These possibilities need to be examined experimentally.

One of the major mechanisms by which ANG II influences neuronal function is by modulating voltage-gated Ca^{2+} currents (19). Our findings indicate that ANG II increases L-type Ca^{2+} currents via AT_1 receptors and NADPH oxidase but that the effect is more marked in female than in male rats. The enhancement of the Ca^{2+} current induced by ANG II in female RVLM bulbospinal neurons is observed only for the dihydropyridine-sensitive L-type Ca^{2+} current and not for the transient Ca^{2+} current. Several possible explanations can be advanced for the sex difference in the ANG II-induced Ca^{2+} current in RVLM neurons. First, AT_1 receptor signaling could induce more ROS in female than in male RVLM neurons. This is unlikely, however, since ANG II-induced ROS production is identical in female and male RVLM neurons. Alternatively, ANG II-induced potentiation of Ca^{2+} currents could be independent of NADPH oxidase-derived ROS, and could be mediated by other signaling pathways initiated by the AT_1 receptor. For example, AT_1 receptor-induced protein kinase C or protein kinase A activation could modulate L-type Ca^{2+} channels (24). This is also unlikely, because gp91ds-tat blocks all ANG II-induced L-type Ca^{2+} currents in female RVLM bulbospinal neurons. Finally, the density of L-type Ca^{2+} channels on RVLM neurons could be greater in females than in males. This possibility is supported by studies in spinal cord motor neurons that exhibit greater L-type Ca^{2+} currents in females than in males (31) and by our finding that application of the L-type Ca^{2+} channel activator Bay K 8644 elicits larger Ca^{2+} currents in female neurons.

Perspectives and Significance

We have thus demonstrated that AT_1 receptors in TH-containing neurons of the RVLM are more abundant in female than in male rats, an increase associated with a reduction in the key NADPH oxidase subunit p47. ANG II produces similar increases in ROS production in RVLM bulbospinal neurons of female and male rats, but the associated enhancement in the L-type Ca^{2+} current is more marked in females than in males. The functional significance of increased L-type Ca^{2+} currents in females remains to be defined. Potentiated L-type Ca^{2+} currents could increase neuronal excitability due to the depolarizing effect of Ca^{2+} influx, potentially affecting sympathetic outflow. Alternatively, excitability could be decreased by activation of Ca^{2+}-activated K^+ channels. In addition, L-type Ca^{2+} channels participate in gene expression, synaptic plasticity, and cell survival (29). Therefore, increased L-type Ca^{2+} currents in females could also lead to a greater potential for plasticity within central autonomic networks. These issues need to be explored in future studies. In summary, these findings unveil previously unrecognized sex differences in ANG II receptor expression and signaling in central autonomic neurons that are critically involved in controlling the cardiovascular system.

GRANT

This study was supported by National Heart, Lung, and Blood Institute Grant HL-18974 and National Institute of Aging Grants AG-16765 and AG-028051.

Acknowledgments

We thank Justin Kievets and Katherine Mitterling for technical assistance.

Notes

The costs of publication of this article were defrayed in part by the payment of page charges. The article must therefore be hereby marked "*advertisement*" in accordance with 18 U.S.C. Section 1734 solely to indicate this fact.

REFERENCES

1. Albert CM, McGovern BA, Newell JB, Ruskin JN. Sex differences in cardiac arrest survivors. *Circulation* 93: 1170–1176, 1996. [PubMed: 8653838]

2. Allen AM, Dosanjh JK, Erac M, Dassanayake S, Hannan RD, Thomas WG. Expression of constitutively active angiotensin receptors in the rostral ventrolateral medulla increases blood pressure. *Hypertension* 47: 1054–1061, 2006. [PubMed: 16618838]

3. Averill DB, Tsuchihashi T, Khosla MC, Ferrario CM. Losartan, nonpeptide angiotensin II-type 1 (AT_1) receptor antagonist, attenuates pressor and sympathoexcitatory responses evoked by angiotensin II and L-glutamate in rostral ventrolateral medulla. *Brain Res* 665: 245–252, 1994. [PubMed: 7895060]

4. Card JP, Sved JC, Craig B, Raizada M, Vazquez J, Sved AF. Efferent projections of rat rostroventrolateral medulla C1 catecholamine neurons: Implications for the central control of cardiovascular regulation. *J Comp Neurol* 499: 840–859, 2006. [PubMed: 17048222]

5. Carey RM Update on the role of the AT_2 receptor. *Curr Opin Nephrol Hypertens* 14: 67–71, 2005. [PubMed: 15586018]

6. Chakraborty TR, Hof PR, Ng L, Gore AC. Stereologic analysis of estrogen receptor-α (ER-α) expression in rat hypothalamus and its regulation by aging and estrogen. *J Comp Neurol* 466: 409–421, 2003. [PubMed: 14556297]

7. Chan SH, Hsu KS, Huang CC, Wang LL, Ou CC, Chan JY. NADPH oxidase-derived superoxide anion mediates angiotensin II-induced pressor effect via activation of p38 mitogen-activated protein kinase in the rostral ventrolateral medulla. *Circ Res* 97: 772–780, 2005. [PubMed: 16151022]

8. Chan SH, Wang LL, Tseng HL, Chan JY. Upregulation of AT1 receptor gene on activation of protein kinase Cβ/nicotinamide adenine dinucleotide diphosphate oxidase/ERK1/2/c-fos signaling cascade mediates long-term pressor effect of angiotensin II in rostral ventrolateral medulla. *J Hypertens* 25: 1845–1861, 2007. [PubMed: 17762649]

9. Dampney RA Functional organization of central pathways regulating the cardiovascular system. *Physiol Rev* 74: 323–364, 1994. [PubMed: 8171117]

10. Gao L, Wang W, Li YL, Schultz HD, Liu D, Cornish KG, Zucker IH. Sympathoexcitation by central ANG II: roles for AT1 receptor upregulation and NAD(P)H oxidase in RVLM. *Am J Physiol Heart Circ Physiol* 288: H2271–H2279, 2005. [PubMed: 15637113]

11. Girouard H, Lessard A, Capone C, Milner TM, Iadecola C. The neurovascular dysfunction induced by angiotensin II in the mouse neocortex is sexually dimorphic. *Am J Physiol Heart Circ Physiol* 294: H156–H163, 2008. [PubMed: 17982007]

12. Glass MJ, Huang J, Oselkin M, Tarsitano MJ, Wang G, Iadecola C, Pickel VM. Subcellular localization of nicotinamide adenine dinucleotide phosphate oxidase subunits in neurons and astroglia of the rat medial nucleus tractus solitarius: relationship with tyrosine hydroxylase immunoreactive neurons. *Neuroscience* 143: 547–564, 2006. [PMCID: PMC1808229] [PubMed: 17027166]

13. Gore AC, Oung T, Woller MJ. Age-related changes in hypothalamic gonadotropin-releasing hormone and *N*-methyl-d-aspartate receptor gene expression, and their regulation by oestrogen, in the female rat. *J Neuroendocrinol* 14: 300–309, 2002. [PubMed: 11963827]

14. Grady D, Herrington D, Bittner V, Blumenthal R, Davidson M, Hlatky M, Hsia J, Hulley S, Herd A, Khan S, Newby LK, Waters D, Vittinghoff E, Wenger N. Cardiovascular disease outcomes during 6.8 years of hormone therapy: Heart and Estrogen/Progestin Replacement Study follow-up (HERS II). *JAMA* 288: 49–57, 2002. [PubMed: 12090862]

15. Guyenet PG The sympathetic control of blood pressure. *Nat Rev Neurosci* 7: 335–346, 2006. [PubMed: 16760914]

16. Guyenet PG, Haselton JR, Sun MK. Sympathoexcitatory neurons of the rostroventrolateral medulla and the origin of the sympathetic vasomotor tone. *Prog Brain Res* 81: 105–116, 1989. [PubMed: 2616776]

17. Hirooka Y, Potts PD, Dampney RA. Role of angiotensin II receptor subtypes in mediating the sympathoexcitatory effects of exogenous and endogenous angiotensin peptides in the rostral ventrolateral medulla of the rabbit. *Brain Res* 772: 107–114, 1997. [PubMed: 9406962]

18. Hsu SM, Raine L, Fanger H. Use of avidin-biotin-peroxidase complex (ABC) in immunoperoxidase techniques: a comparison between ABC and unlabeled antibody (PAP) procedures. *J Histochem Cytochem* 29: 557–580, 1981. [PubMed: 6166661]

19. Huang CC, Chan SH, Hsu KS. 3-Morpholinylsydnonimine inhibits glutamatergic transmission in rat rostral ventrolateral medulla via peroxynitrite formation and adenosine release. *Mol Pharmacol* 66: 492–501, 2004. [PubMed: 15322240]

20. Huang J, Hara Y, Anrather J, Speth RC, Iadecola C, Pickel VM. Angiotensin II subtype 1A (AT1A) receptors in the rat sensory vagal complex: subcellular localization and association with endogenous angiotensin. *Neuroscience* 122: 21–36, 2003. [PubMed: 14596846]

21. Infanger DW, Sharma RV, Davisson RL. NADPH oxidases of the brain: distribution, regulation, and function. *Antioxid Redox Signal* 8: 1583–1596, 2006. [PubMed: 16987013]

22. Ishibashi H, Akaike N. Norepinephrine modulates high voltage-activated calcium channels in freshly dissociated rat nucleus tractus solitarii neurons. *Neuroscience* 68: 1139–1146, 1995. [PubMed: 8544988]

23. Johren O, Sanvitto GL, Egidy G, Saavedra JM. Angiotensin II AT_{1A} receptor mRNA expression is induced by estrogen-progesterone in dopaminergic neurons of the female rat arcuate nucleus. *J Neurosci* 17: 8283–8292, 1997. [PMCID: PMC6573735] [PubMed: 9334403]

24. Kamp TJ, Hell JW. Regulation of cardiac L-type calcium channels by protein kinase A and protein kinase C. *Circ Res* 87: 1095–1102, 2000. [PubMed: 11110765]

25. Kazama K, Anrather J, Zhou P, Girouard H, Frys K, Milner TA, Iadecola C. Angiotensin II impairs neurovascular coupling in neocortex through NADPH oxidase-derived radicals. *Circ Res* 95: 1019–1026, 2004. [PubMed: 15499027]

26. Kishi T, Hirooka Y, Kimura Y, Ito K, Shimokawa H, Takeshita A. Increased reactive oxygen species in rostral ventrolateral medulla contribute to neural mechanisms of hypertension in stroke-prone spontaneously hypertensive rats. *Circulation* 109: 2357–2362, 2004. [PubMed: 15117836]

27. Korner PI *Essential Hypertension and Its Causes.* New York: Oxford University Press, 2007.

28. Li YW, Guyenet PG, Bayliss DA. Voltage-dependent calcium currents in bulbospinal neurons of neonatal rat rostral ventrolateral medulla: modulation by α_2-adrenergic receptors. *J Neurophysiol* 79: 583–594, 1998. [PubMed: 9463423]

29. Lipscombe D, Helton TD, Xu W. L-type calcium channels: the low down. *J Neurophysiol* 92: 2633–2641, 2004. [PubMed: 15486420]

30. Madden CJ, Sved AF. Cardiovascular regulation after destruction of the C1 cell group of the rostral ventrolateral medulla in rats. *Am J Physiol Heart Circ Physiol* 285: H2734–H2748, 2003. [PubMed: 12933337]

31. Manabe T, Araki I, Takahashi T, Kuno M. Membrane currents recorded from sexually dimorphic motoneurones of the bulbocavernosus muscle in neonatal rats. *J Physiol* 440: 419–435, 1991. [PMCID: PMC1180160] [PubMed: 1804970]

32. Matthews KA, Kuller LH, Sutton-Tyrrell K, Chang YF. Changes in cardiovascular risk factors during the perimenopause and postmenopause and carotid artery atherosclerosis in healthy women. *Stroke* 32: 1104–1111, 2001. [PubMed: 11340217]

33. Milner TA, Drake CT, Aicher SA. Cellular relations between μ-opioid receptive, GABAergic and reticulospinal neurons in the rostral ventrolateral medulla. *Brain Res* 917: 1–14, 2001. [PubMed: 11602225]

34. Oliveira-Sales EB, Dugaich AP, Carillo BA, Abreu NP, Boim MA, Martins PJ, D'Almeida V, Dolnikoff MS, Bergamaschi CT, Campos RR. Oxidative stress contributes to renovascular hypertension. *Am J Hypertens* 21: 98–104, 2008. [PubMed: 18091751]

35. Ouchi Y, Share L, Crofton JT, Iitake K, Brooks DP. Sex difference in the development of deoxycorticosterone-salt hypertension in the rat. *Hypertension* 9: 172–177, 1987. [PubMed: 3818014]

36. Pamidimukkala J, Hay M. 17β-Estradiol inhibits angiotensin II activation of area postrema neurons. *Am J Physiol Heart Circ Physiol* 285: H1515–H1520, 2003. [PubMed: 12829428]

37. Peters A, Palay SL, Webster HD. *The Fine Structure of the Nervous System: the Neurons and Supporting Cells.* Philadelphia, PA: Saunders, 1991.

38. Peterson JR, Sharma RV, Davisson RL. Reactive oxygen species in the neuropathogenesis of hypertension. *Curr Hypertens Rep* 8: 232–241, 2006. [PubMed: 17147922]

39. Phillips JK, Goodchild AK, Dubey R, Sesiashvili E, Takeda M, Chalmers J, Pilowsky PM, Lipski J. Differential expression of catecholamine biosynthetic enzymes in the rat ventrolateral medulla. *J Comp Neurol* 432: 20–34, 2001. [PubMed: 11241375]

40. Pierce JP, Graustein B, Iadecola C, Milner TA. *Significantly Higher Levels of Labeling for the NADPH Oxidase Subunit, p47, are Displayed in C1 Neurons in the Rostral Ventrolateral Medulla of Male Versus Female Rats.* San Diego, CA: Society for Neuroscience, 2007.

41. Pierce JP, Kurucz OS, Milner TA. Morphometry of a peptidergic transmitter system: dynorphin B-like immunoreactivity in the rat hippocampal mossy fiber pathway before and after seizures. *Hippocampus* 9: 255–276, 1999. [PubMed: 10401641]

42. Pierce JP, Melton J, Punsoni M, McCloskey DP, Scharfman HE. Mossy fibers are the primary source of afferent input to ectopic granule cells that are born after pilocarpine-induced seizures. *Exp Neurol* 196: 316–331, 2005. [PMCID: PMC1431686] [PubMed: 16342370]

43. Pierce JP, Punsoni M, McCloskey DP, Scharfman HE. Mossy cell axon synaptic contacts on ectopic granule cells that are born following pilocarpine-induced seizures. *Neurosci Lett* 422: 136–140, 2007. [PMCID: PMC3119631] [PubMed: 17611032]

44. Reckelhoff JF Gender differences in the regulation of blood pressure. *Hypertension* 37: 1199–1208, 2001. [PubMed: 11358929]

45. Romeo RD Puberty: a period of both organizational and activational effects of steroid hormones on neurobehavioural development. *J Neuroendocrinol* 15: 1185–1192, 2003. [PubMed: 14636181]

46. Ross CA, Ruggiero DA, Joh TH, Park DH, Reis DJ. Rostral ventrolateral medulla: selective projections to the thoracic autonomic cell column from the region containing C1 adrenaline neurons. *J Comp Neurol* 228: 168–185, 1984. [PubMed: 6480910]

47. Ross CA, Ruggiero DA, Park DH, Joh TH, Sved AF, Fernandez-Pardal J, Saavedra JM, Reis DJ. Tonic vasomotor control by the rostral ventrolateral medulla: effect of electrical or chemical stimulation of the area containing C1 adrenaline neurons on arterial pressure, heart rate, and plasma catecholamines and vasopressin. *J Neurosci* 4: 474–494, 1984. [PMCID: PMC6564896] [PubMed: 6699683]

48. Santos RA, Ferreira AJ. Angiotensin-(1-7) and the renin-angiotensin system. *Curr Opin Nephrol Hypertens* 16: 122–128, 2007. [PubMed: 17293687]

49. Schreihofer AM, Stornetta RL, Guyenet PG. Regulation of sympathetic tone and arterial pressure by rostral ventrolateral medulla after depletion of C1 cells in rat. *J Physiol* 529: 221–236, 2000. [PMCID: PMC2270165] [PubMed: 11080264]

50. Sesack SR, Pickel VM. Dual ultrastructural localization of enkephalin and tyrosine hydroxylase immunoreactivity in the rat ventral tegmental area: multiple substrates for opiate-dopamine interactions. *J Neurosci* 12: 1335–1350, 1992. [PMCID: PMC6575793] [PubMed: 1348271]

51. Sisk CL, Zehr JL. Pubertal hormones organize the adolescent brain and behavior. *Front Neuroendocrinol* 26: 163–174, 2005. [PubMed: 16309736]

52. Sourander L, Rajala T, Raiha I, Makinen J, Erkkola R, Helenius H. Cardiovascular and cancer morbidity and mortality and sudden cardiac death in postmenopausal women on oestrogen replacement therapy (ERT). *Lancet* 352: 1965–1969, 1998. [PubMed: 9872245]

53. Sun C, Sellers KW, Sumners C, Raizada MK. NAD(P)H oxidase inhibition attenuates neuronal chronotropic actions of angiotensin II. *Circ Res* 96: 659–666, 2005. [PubMed: 15746442]

54. Sved AF, Mancini DL, Graham JC, Schreihofer AM, Hoffman GE. PNMT-containing neurons of the C1 cell group express c-fos in response to changes in baroreceptor input. *Am J Physiol Regul Integr Comp Physiol* 266: R361–R367, 1994. [PubMed: 8141390]

55. Swanson LW *Brain Maps: Structure of the Rat Brain.* New York: Elsevier, 1999.

56. Tucker DC, Saper CB, Ruggiero DA, Reis DJ. Organization of central adrenergic pathways: I. Relationships of ventrolateral medullary projections to the hypothalamus and spinal cord. *J Comp Neurol* 259: 591–603, 1987. [PubMed: 2885348]

57. Wang G, Anrather J, Glass MJ, Tarsitano MJ, Zhou P, Frys KA, Pickel VM, Iadecola C. Nox2, Ca^{2+}, and protein kinase C play a role in angiotensin II-induced free radical production in nucleus tractus solitarius. *Hypertension* 48: 482–489, 2006. [PubMed: 16894058]

58. Wang G, Anrather J, Huang J, Speth RC, Pickel VM, Iadecola C. NADPH oxidase contributes to angiotensin II signaling in the nucleus tractus solitarius. *J Neurosci* 24: 5516–5524, 2004. [PMCID: PMC6729325] [PubMed: 15201324]

59. Wang G, Drake CT, Rozenblit M, Zhou P, Alves SE, Herrick SP, Hayashi S, Warrier S, Iadecola C, Milner TA. Evidence that estrogen directly and indirectly modulates C1 adrenergic bulbospinal neurons in the rostral ventrolateral medulla. *Brain Res* 1094: 163–178, 2006. [PubMed: 16696957]

60. Wang G, Zhou P, Repucci MA, Golanov EV, Reis DJ. Specific actions of cyanide on membrane potential and voltage-gated ion currents in rostral ventrolateral medulla neurons in rat brainstem slices. *Neurosci Lett* 309: 125–129, 2001. [PubMed: 11502361]

61. Wang H, Cuzon VC, Pickel VM. Postnatal development of μ-opioid receptors in the rat caudate-putamen nucleus parallels asymmetric synapse formation. *Neuroscience* 118: 695–708, 2003. [PubMed: 12710977]

62. Xue B, Pamidimukkala J, Lubahn DB, Hay M. Estrogen receptor-α mediates estrogen protection from angiotensin II-induced hypertension in conscious female mice. *Am J Physiol Heart Circ Physiol* 292: H1770–H1776, 2007. [PubMed: 17142339]

63. Zimmerman MC, Lazartigues E, Sharma RV, Davisson RL. Hypertension caused by angiotensin II infusion involves increased superoxide production in the central nervous system. *Circ Res* 95: 210–216, 2004. [PubMed: 15192025]

64. Zimmerman MC, Sharma RV, Davisson RL. Superoxide mediates angiotensin II-induced influx of extracellular calcium in neural cells. *Hypertension* 45: 717–723, 2005. [PubMed: 15699459]

Figures and Tables

Fig. 1.

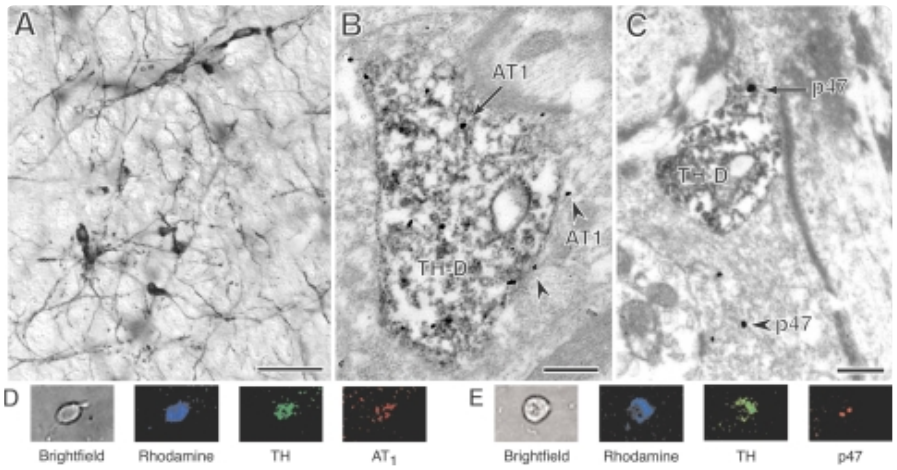

By light microscopy, tyrosine hydroxylase (TH)-labeled somata and dendrites (*A*) are clearly visible in the RVLM (bar, 40 μm) of a postnatal *day 23* (P23) female. By electron microscopy, TH-immunoperoxidase (TH-ImP)-labeled dendrites (TH-D) often displayed immunogold (ImG) labeling (arrows) for the AT_1 receptor (AT_1) (*B*), or the p47 subunit (p47) (*C*) (bars, 0.5 μm). ImG labeling for both the AT_1 receptor and p47 subunit was also frequently found in non-TH-positive processes, such as AT_1-ImG labeling of a glial process (arrowheads) adjacent to a TH-positive dendrite (*B*) and p47-ImG labeling (arrowhead) of a presynaptic terminal (*C*). TH and AT_1 receptor (*D*) or p47 subunit (*E*) immunoreactivities are coexpressed in the same rhodamine-labeled RVLM neuron from a female rat.

Fig. 2.

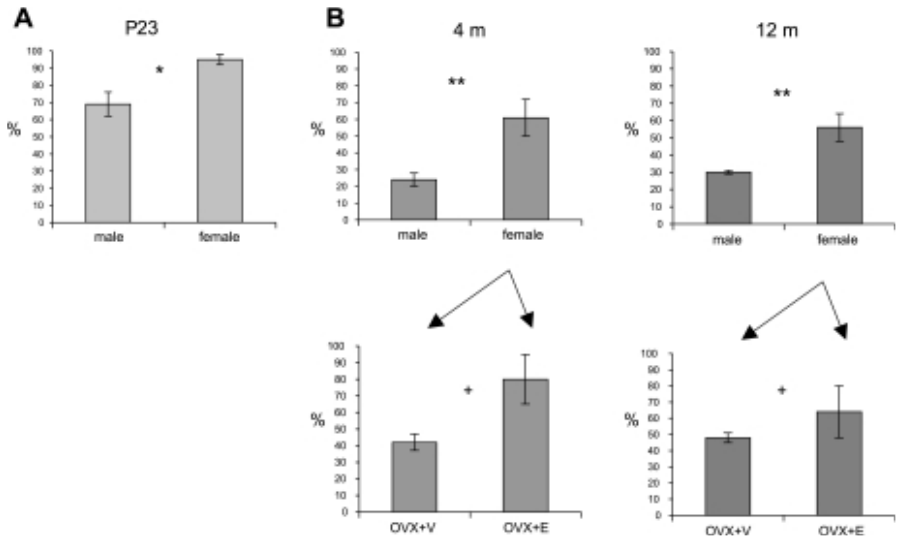

Histograms of the relative density of AT_1-ImG particle labeling of TH-positive dendritic profiles in the RVLM of P23 (*A*), and 4- and 12-mo-old (*B*) rats. Since the data presented in *A* and *B* was obtained from tissue that had been processed separately, values are normalized to the highest value in each, to facilitate comparison (see text for original values). At P23 (*A*), females displayed significantly higher levels of AT_1-ImG labeling than those of males. At 4 and 12 mo (*B*), females also displayed significantly higher levels of AT_1-ImG labeling than those of males, and ovariectomized+estradiol (OVX+E) females had significantly higher levels than ovariectomized+vehicle (OVX+V) females, while there were no significant difference relating to age. **P* = 0.03, ***P* = 0.008, +*P* = 0.04.

Fig. 3.

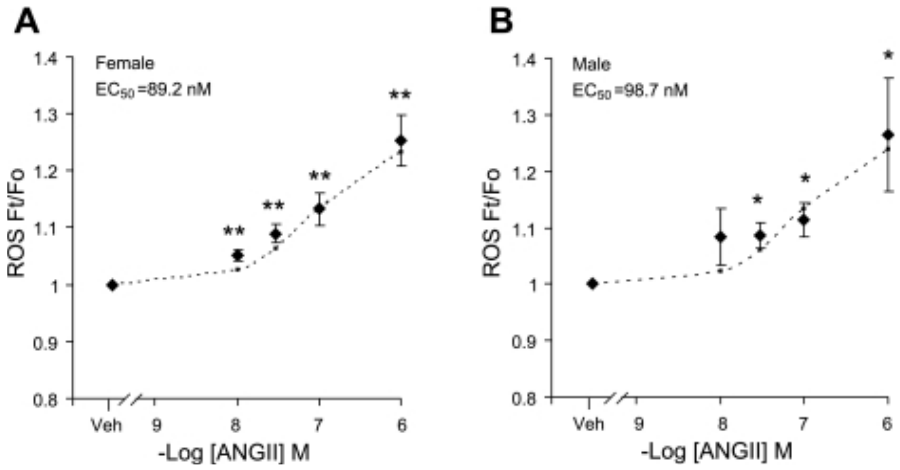

Comparison of the dose-response curves of ANG II's effects on reactive oxygen species (ROS) production in RVLM neurons of female and male rats. *A*: ANG II dose-dependently induced an increase in ROS production in retrogradely labeled RVLM bulbospinal neurons of female rats (EC_{50} = 89.2 nmol/l; vehicle = 10, ANG II: 10 nmol/l = 5, 30 nmol/l = 5, 100 nmol/l = 5, 1,000 nmol/l = 9). *B*: ANG II dose-dependently induced an increase in ROS production in retrogradely labeled RVLM bulbospinal neurons of male rats (EC_{50} = 98.7 nmol/l; vehicle = 14, ANG II: 10 nmol/l = 4, 30 nmol/l = 4, 100 nmol/l = 5, 1,000 nmol/l = 8). The dotted curves are fitted values calculated from the equation $y = \min + (\max - \min)/[1 + (x/EC_{50})^{Hillslope}]$. Ft, fluorescence following the application of ANG II at a given time Fo, baseline fluorescence of the same cell immediately before application of ANG II. **P* < 0.05 and ***P* < 0.01 vs. vehicle.

Fig. 4.

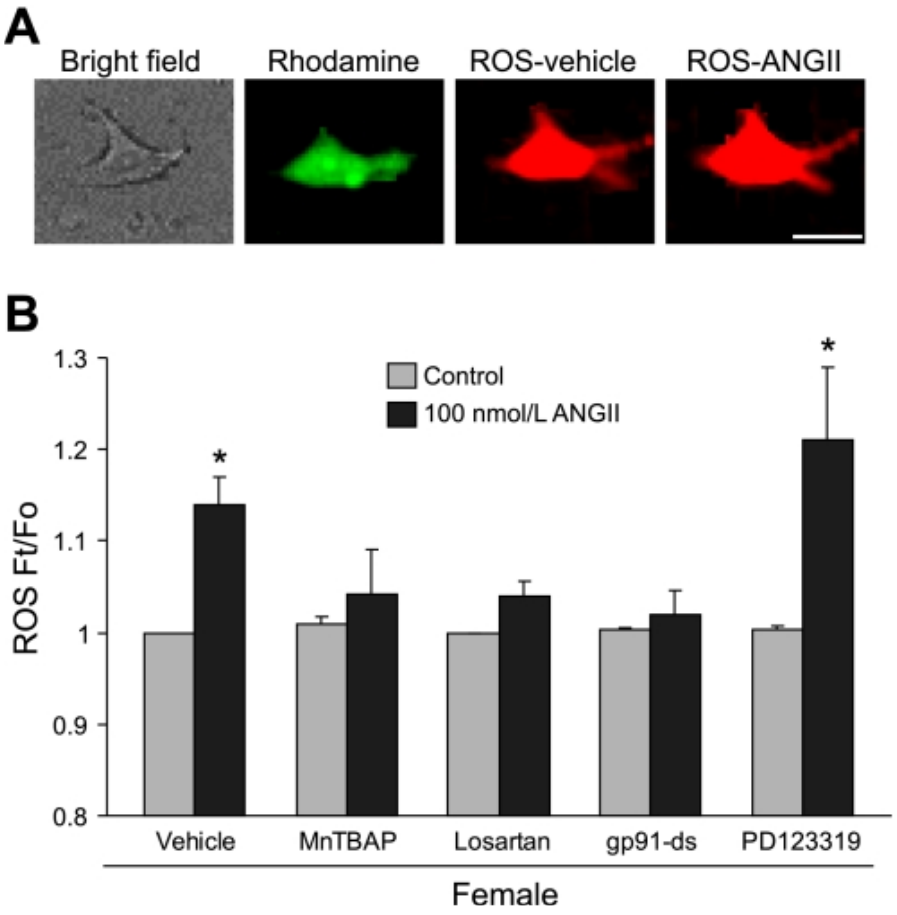

ANG II induces ROS production in female RVLM neurons. *A*: representative images show the ANG II-induced increase in ethidium bromide fluorescence intensity in a rhodamine-labeled RVLM neuron (bars, 10 μm). *B*: histogram illustrating the effect of vehicle (n = 5), Mn(III)tetrakis(4-benzoic acid)porphyrin chloride (MnTBAP; 30 μmol/l; n = 6), losartan (10 μmol/l; n = 4), gp91ds-tat (gp91-ds, 1 μmol/l; n = 7), and PD123319 (30 μmol/l; n = 5) on the increase in ROS (Ft/Fo) induced by ANG II (100 nmol/l) in RVLM bulbospinal neurons. *P < 0.05 vs. control.

Fig. 5.

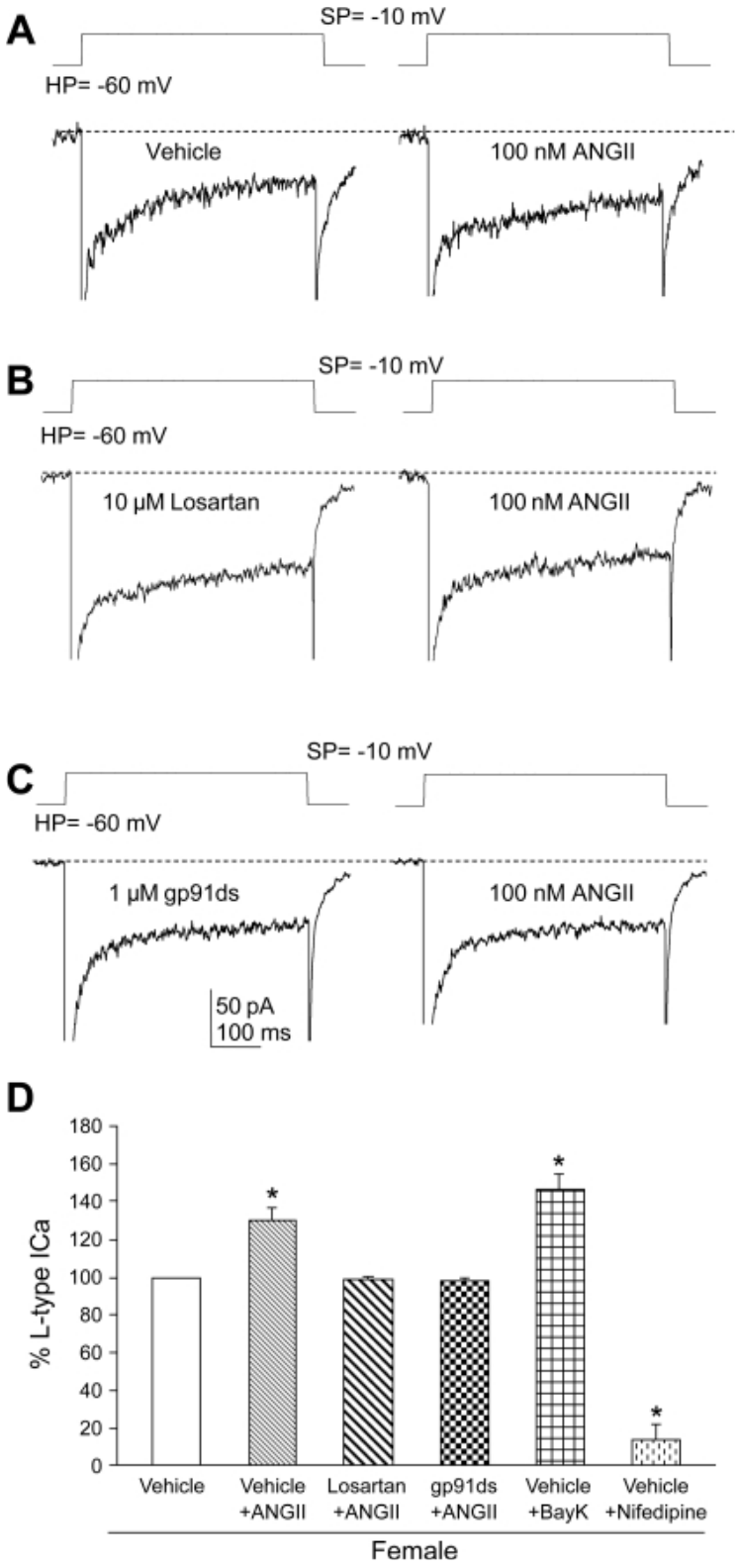

ANG II potentiates long-lasting (L-type) Ca^{2+} currents in female RVLM neurons. *A*: whole-cell Ca^{2+} currents from the same RVLM neuron in the presence of vehicle and ANG II. *B*: whole-cell Ca^{2+} currents from the same RVLM neuron in the presence of losartan and losartan + ANG II. *C*: whole-cell Ca^{2+} currents from the same RVLM neuron in the presence of gp91ds-tat and gp91ds-tat + ANG II. *D*: histogram illustrating the effects of vehicles (n = 6), losartan (10 μmol/l; n = 4), gp91ds-tat (gp91ds, 1 μmol/l; n = 4), Bay K 8644 (Bay K 8644, 1 μmol/l; n = 4), and nifedipine (1 μmol/l; n = 4) on the increase in L-type Ca^{2+} currents induced by ANG II. *P < 0.05 vs. vehicles. SP, stepping potential; HP, holding potential.

Fig. 6.

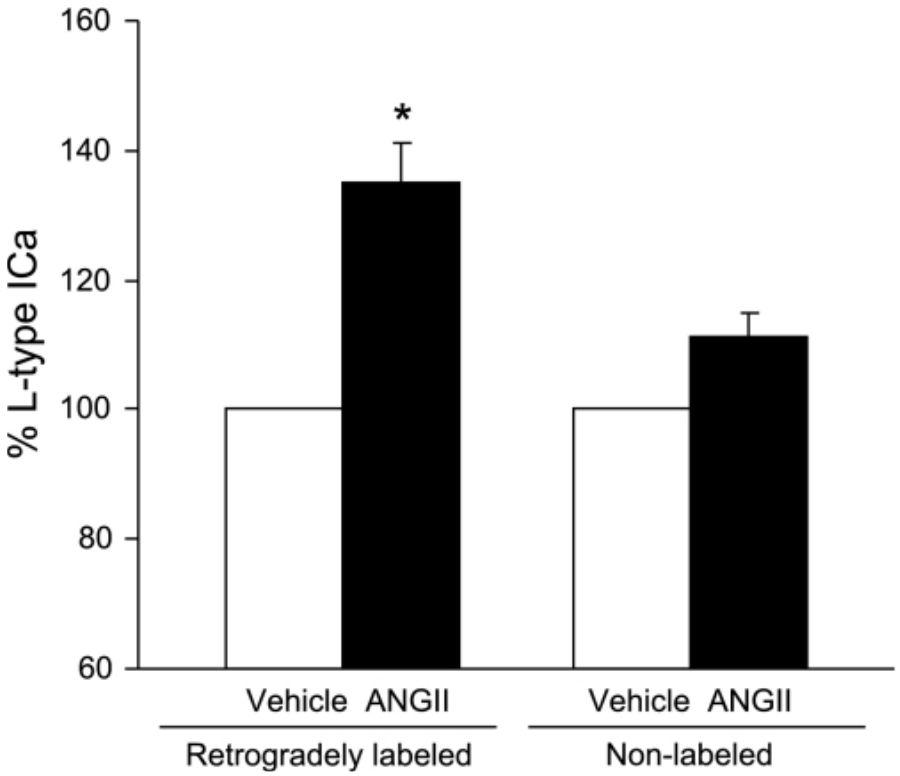

Comparison of the effects of ANG II on Ca^{2+} currents in retrogradely labeled and nonlabeled neurons of the RVLM in female rats. ANG II (100 nmol/l) induced a significant increase in the L-type Ca^{2+} current (I_{Ca}) in retrogradely labeled RVLM bulbospinal neurons ($n = 6$). In contrast, ANG II (100 nmol/l) did not have a significant effect on the L-type Ca^{2+} current in nonlabeled neurons isolated from the RVLM ($n = 4$). *$P < 0.05$ vs. vehicle.

Fig. 7.

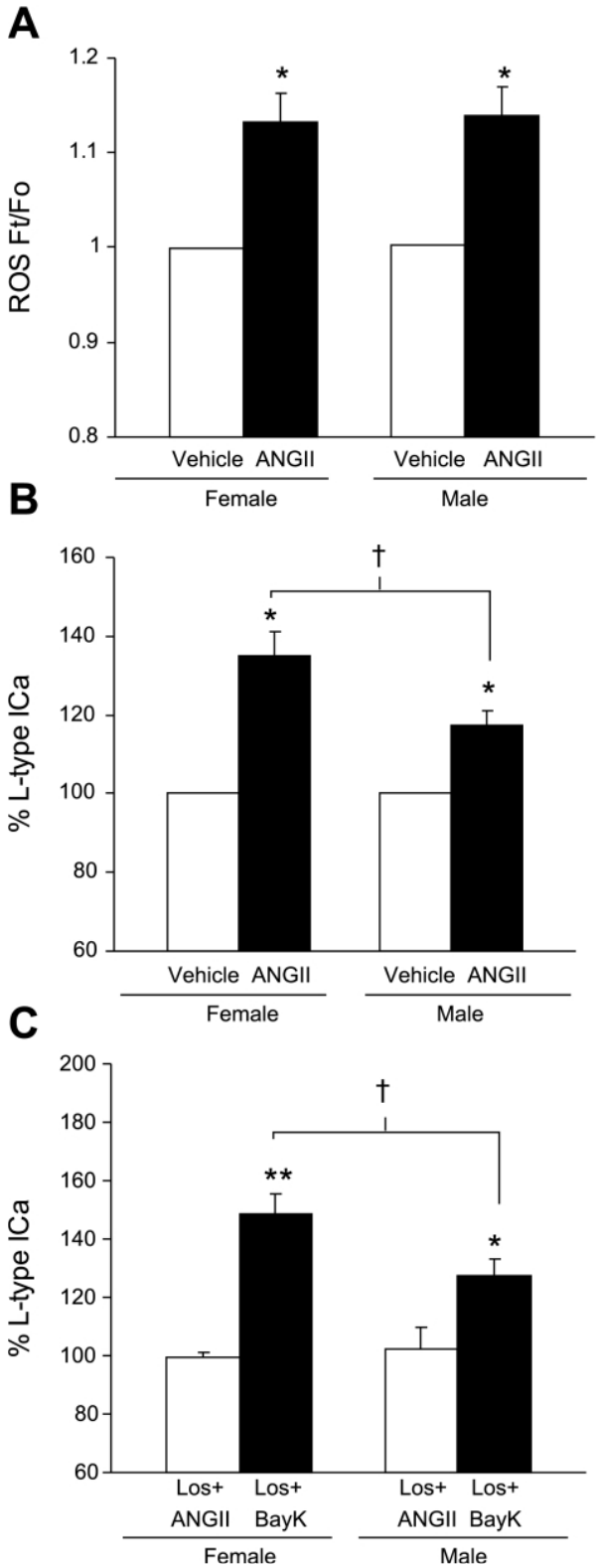

Comparison of ANG II-induced ROS production and Ca^{2+} currents between male and female rat RVLM neurons. *A*: ANG II (100 nmol/l) induced a comparable increase in ROS in RVLM bulbospinal neurons from female (n = 5, same as vehicle in Fig. 4*B*) and male (n = 5) rats. *B*: ANG II (100 nmol/l) induced a greater increase in the L-type Ca^{2+} current in RVLM neurons from female rats (n = 6), compared with male rats (n = 6). *C*: ANG II (100 nmol/l)-induced increase in the L-type Ca^{2+} cur-

rent was equivalently inhibited by losartan (10 μmol/l) in male and female RVLM neurons (n = 4). In the presence of losartan (10 μmol/l), Bay K 8644 (1 μmol/l) increased the L-type Ca^{2+} current to a greater extent in female (n = 4) than in male (n = 5) RVLM neurons. *P < 0.05 and **P < 0.01 *vs*. vehicle; †P < 0.05.